fibers

MDPI

Article

Petrography, Geochemistry and Mineralogy of Serpentinite Rocks Exploited in the Ophiolite Units at the Calabria-Basilicata Boundary, Southern Apennine (Italy)

Giovanna Rizzo [1], Roberto Buccione [1,*], Marilena Dichicco [1], Rosalda Punturo [2,3] and Giovanni Mongelli [1]

[1] Department of Sciences, University of Basilicata, Via dell'Ateneo Lucano, 10 85100 Potenza, Italy; giovanna.rizzo@unibas.it (G.R.); marilena.dichicco@libero.it (M.D.); giovanni.mongelli@unibas.it (G.M.)
[2] Department di Scienze Biologiche, Geologiche e Ambientali, University of Catania, Corso Italia, 57 95129 Catania, Italy; punturo@unict.it
[3] Institute of Environmental Geology and Geoengineering (IGAG-CNR), Piazzale Aldo Moro, 7 00185 Roma, Italy
* Correspondence: roberto.buccione@unibas.it

Abstract: A multi-analytical study on serpentinites in the ophiolite units (Calabria-Basilicata boundary, southern Apennines) was carried out on samples collected from a serpentinite quarry, locally called "Pietrapica", which sitsin the Pollino UNESCO Global Geopark. Optical microscopy observations revealed the petrographic characteristics, ICP-MS was used to assess the chemical composition while EMPA mineral chemistry, Raman spectroscopy and X-Ray Powder Diffraction and were used altogether to trace the mineral composition of the rocks. Petrography revealed that serpentinites from Pietrapica quarry are essentially composed of serpentine group minerals, amphibole and carbonate minerals with lower abundances of talc and Cr-spinel. Raman spectroscopy and X-ray powder diffraction analysis clearly allowed to establish that carbonate minerals, serpentine and amphibole-like minerals, are the dominant phases, followed by 2:1 phyllosilicate. Electron probe microanalyses were carried out on different minerals in serpentinites samples including serpentine, amphibole, chlorite, clinopyroxene, magnetite, talc, quartz and titanite which are often associated with carbonate veins. Bulk geochemistry is dominated by major oxides SiO_2, MgO and Fe_2O_3 while the most abundant trace elements are Ni and Cr. Chemical analysis showed that some heavy metals in the studied serpentinites such as Ni and Cr, are beyond the maximum admissible limits for Italian normative for public, private and residential green as well as for commercial and industrial use representing a potential environmental concern. Anyway, some of these heavy metals have been recently listed by Europe as critical raw materials and therefore, the Pietrapica abandoned quarry could represent a new resource considering their economic potentiality.

Keywords: quarry; serpentinite; ophiolite; Pollino Massif; Southern Apennines

Citation: Rizzo, G.; Buccione, R.; Dichicco, M.; Punturo, R.; Mongelli, G. Petrography, Geochemistry and Mineralogy of Serpentinite Rocks Exploited in the Ophiolite Units at the Calabria-Basilicata Boundary, Southern Apennine (Italy). *Fibers* **2023**, *11*, 81. https://doi.org/10.3390/fib11100081

Academic Editor: Martin J. D. Clift

Received: 13 July 2023
Revised: 31 August 2023
Accepted: 18 September 2023
Published: 23 September 2023

1. Introduction

Ophiolite tectonic units, which testify the occurrence in the past of the oceans subducted/obducted at convergent margins, are a common feature of many orogenic belts. Based on their P-T path, ophiolites can represent well preserved and weakly metamorphosed mantle—crust oceanic sequences as well as by disrupted and fragmented metamorphic lenses embedded in marbles, schists, gneiss and other metamorphic rocks. The P-T-t paths are generally classified into two main types which are the clockwise and anticlockwise P-T-t paths. The clockwise paths, are related to collision origin, and involve high pressures followed by high temperatures while in the anticlockwise P-T-t paths, are usually related to intrusion origin, involving high temperatures before high pressures [1]. The ophiolite sequences, as subaerial witness of oceanic lithosphere, potentially provide fundamental details about the nature and development of extensional processes which

operated in various oceanic-type spreading regimes at crustal and upper mantle depths that cannot be directly examined in the modern oceans. Indeed. although ophiolite emplacement typically results in various extent of deformation and associated metamorphic degree, the multiplicity of stratigraphic levels exposed in ophiolites provides an essential complement to the oceanographic database. The recognition of faults and veins related to subseafloor spreading processes in ophiolites, and their distinction from similar features possibly developed during the orogenic evolution, is of critical importance because ophiolites are employed as analogues for oceanic lithosphere.

Ophiolite complexes that crop out commonly comprise serpentinite sections crosscut by carbonate veins, carbonate-serpentine breccias and serpentine-hosted carbonate deposits, all of which are referred with the general term of ophicalcites. Ophicalcites are found in the Alpine orogenic belt and likely formed in the Tethys Ocean during the Mesozoic [2–6]. A similarity between these ophicalcites has been observed with the basement stockwork system of the LCHF (Lost City hydrothermal field) [7,8], so they were likely formed at low to moderate temperature hydrothermal and tectonic processes in environments of near-ridge or fracture zone or in passive margins during exhumation of subcontinental mantle.

Although the overall physical-chemical conditions associated with formation of these deposits are commonly obscured or obliterated by subsequent recrystallization and metamorphic overprint, the studies of ancient ophicalcites at the scale of the outcrop offer t information on the geometry of fracture networks and fluid pathways which are of paramount importance. Moreover, results from geochemical studies provide information for evaluating the importance of serpentinites as long-term sinks for seawater- derived elements (i.e., C, S, B, H_2O, Mg; [9,10]).

Because of their unique aesthetic features and to their mechanical properties such as tensile strength, flexibility, high thermal stability, serpentinite rocks are extensively used, used as building and construction stones and, for this reason, they have been important natural georesources for many countries where they crop out and may be exploited (e.g., [11–22]). It is worth noting that serpentinite rocks may present concerns related to asbestos minerals that, related to the exploitation process and the "change in service" from the natural outcrops to monuments and buildings, may be released into the environment and pose health issues. For these reasons, it is of crucial importance to assess the occurrence, if any, of asbestos minerals in order to evaluate if the serpentinite rocks from the quarry's rocks can be applied either in construction or conservation-restoration of the architectonic and cultural heritage, and to plan good practices aimed to prevent health risks during excavations and use of serpentinite as stone material. In the southern Apennines, there are several historical quarries that sit on the serpentinite rocks of the ophiolite units, that have been investigated at various extents (e.g., [19,23–25]).

Moreover, it is worth noting that asbestos-bearing serpentinites in the Pollino Massif (Calabria-Basilicata boundary, Southern Apennine, Italy) have been reported at the scale of the outcrop as well as in several active and abandoned quarries, some of which have been investigated (e.g., [26–30]).

In the present work, we present petrographic, mineralogical and geochemical results regarding a suite of studied serpentinite rocks from the Pietrapica quarry. In the area of the Pollino Unesco Global Geopark, serpentinite rocks have been used since long time for several purposes as civil constructions, road building material and building stones. In support of this, it has been observed that serpentinites were used as cement mortars for the construction of the mother church of San Nicola, Episcopia (ad-ministrative district of the city of Potenza). Our study aims to assess whether they can be (re)used properly, as an ornamental stone or as conservation-restoration material. Moreover, knowledge of serpentinite behavior is important in prevention of rock decay processes, as this dimension stone is widely used these days in tiling in several public and private buildings.

2. Geological Framework

The Pollino Massif consists of thrust belts which derived from the deformation of the African passive margin which, between the Oligocene and the Pleistocene, involved the Ligurian ocean ophiolitic lithosphere [31–34]. The Ligurian Complex is composed of two ophiolite-bearing units, the non-metamorphic Calabro-Lucanian Flysch Unit and the metamorphic Frido Unit which were affected by intense tectonic activity [35,36]. During Cretaceous-Paleocene, the Frido Unit experienced low-temperature and high-pressure metamorphism [37–40] (Figure 1).

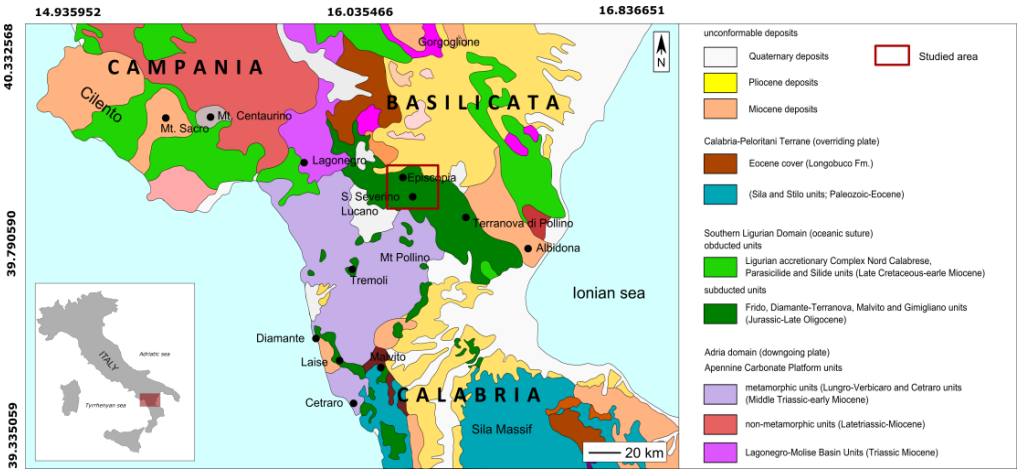

Figure 1. Geological map of Southern Apennines (modified after [39]).

Serpentinites are related with metamorphosed ophiolitic suite where magmatic mafic dykes cut medium to high-grade metamorphic rocks [41]. The ophiolite suites underwent two phases of ocean floor metamorphism [39,41] during which some processes such as ductile deformation, recrystallization and hydrothermal metasomatism promoted the formation of the current mineral assemblage including, the occurrence of fibrous minerals. The serpentinites were classified as cataclastic and massive [25,42,43]. Several cross-cutting fractures were observed, and they are filled by exposed fibrous minerals which can be easily released by water runoff and weathering processes that take place. Two types of fibers have been identified in the studied quarry: (i) large and elongated fibers developed over slickensided surfaces; (ii) very fine-grained fibers forming a network pervading the whole rock [42].

On the other side, the massive serpentinites are weakly fractured and deformed and any exposed fibrous minerals. Either the cataclastic-type and massive serpentinites show similar mineral assemblage consisting of serpentine, tremolite-actinolite, chlorite, magnetite and other Cr-spinels, with minor presence of calcite, dolomite and clay minerals.

3. Sampling and Methods

The serpentinite rocks were collected from the Pietrapica quarry, located at the Calabria-Basilicata boundary, near to San Severino Lucano and Episcopia villages (Basilicata region, Southern Italy) (Figure 2).

Detailed sampling revealed a range of intensely deformed, metamorphosed and metasomatized rocks that testify a protracted history of high strain and fluid-rock interactions. In Pietrapica quarry, the serpentinites are delimited in the upper portion by gneiss, amphibolite and meta granitoids associated with rodingite dykes and in the lower portion by shales, calcschists and meta limestone. The serpentinites show a complex exposure of dark green cataclastic serpentinites (almost always intensely tectonized) with evident slip surface and pseudo-badlands morphology. Moreover, serpentinite lithotypes-hosted talc-rich bodies that are also often associated with quartz and carbonate veins (Figure 3a,b).

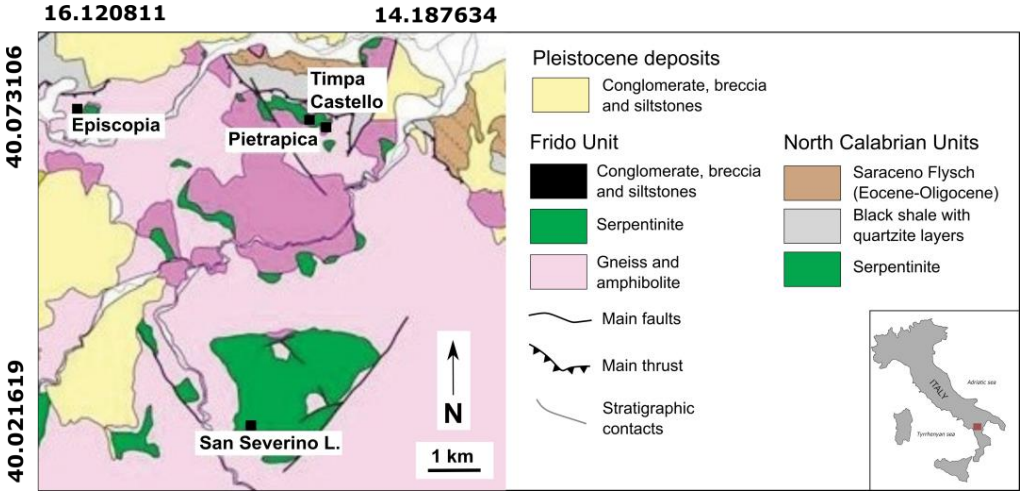

Figure 2. Simplified geological sketch map of the Liguride Complex in the Pollino Massif and location of the sampled area (modified after [42]).

Figure 3. (**a**) Pietrapica quarry; (**b**) Zoom on serpentinites sample.

Petrographic observations, XRPD assessment and Raman spectroscopy were carried out at the Department of Sciences, University of Basilicata (Italy).

The petrographic investigation was made by using a Nikon Alphaphot-2 YS2 optical microscope on thin sections prepared from the specimens.

XRPD analyses were performed on specimens obtained by either bulk rock and vein infill, by using a Siemens D5000 equipment with CuKα radiation, 40 kV and 32 mA.

The powdering of the samples for chemical and mineralogical analysis was made by using a Retsch RS 100 planetary mill equipped with agate jars and agate milling balls. Analysis were performed between 0° and 70° 2θ, using a step size of 0.02° and scan speed of 2 s.

Raman analysis was made using a Horiba Jobin-Yvon LabRam HR800 spectrometer on hermetically sealed rock slabs. The spectrometer is equipped with a HeNe laser source (wavelength of 633 nm), a CCD detector and an edge filter excluding the shift below 150 cm^{-1}. The instrument was calibrated by checking the position of the Si band at $\pm$520.7 cm^{-1}. The laser has a potential of 20 mV and observations were made by using optical microscope Olympus with objective of 10X, 50X and 100X. An average of 5 acquisitions of 10 s permitted the optimization of the signal/noise ratio.

Mineral chemistry were determined by electron microprobe (EMP) analyses using an EMP JEOL Superprobe JXA-8900 M at the Centro Nacional de Microscopía Electrónica (CNME) of the Universidad Complutense (Madrid, Spain). Silicate and oxide analyses were performed at 15 kV accelerating voltage conditions, an electron beam current of 20 nA, with a beam diameter of 5 µm. For carbonate minerals, a voltage of 20 kV, an electron current of 10 nA, and a beam diameter of 5 µm were used. All elements were analyzed for a 15 s time span. Several minerals were used as standard for chemical elements as follows: sillimanite was used for Al, albite was used for Si and Na, almandine was used for Mn and Fe, kaersutite was used for Mg, Ti and Ca, microcline was used for K, fluorapatite was used for P, Ca, F, Cl and Ni, Cr pure metals. The uncertainties for mayor and minor elements range from ±0.8% to ±5%. Major and trace elements were determined by using ICP and ICPMS analysis at Activation Laboratories (Ancaster, Canada), after sample powders digestion with acid attack (HF, $HClO_4$, HNO_3 and HCl). A 0.25-g sample powder was firstly digested in hydrofluoric acid, then with a mixture of nitric and perchloric acids. Then samples were heated in several cycles using controlled heating that took the samples to incipient dryness. The samples were brought back into solution using aqua regia and then analyzed using Varian ICP and PerkinElmer Sciex ELAN 9000 spectrometer. Analytical uncertainties are less than ± 5% while elements at ≤10 mg/kg concentrations have uncertainties of ±5–10%. Finally, the L.O.I. (Loss On Ignition) was estimated after heating at 950 °C.

4. Results

4.1. Petrography

Serpentinite rocks from the Pietrapica quarry are essentially composed of serpentine group minerals, amphibole, and carbonate minerals with minor talc and Cr-spinel. Sometimes, serpentine minerals preserve the original crystal habit of the protolith mafic minerals. Chrysotile polymorph occurs as elongated fibrous veinlets cross-cutting the serpentine massive matrix, indicating protracted serpentinization (Figure 4a). Antigorite crystallization showing irregular patchy texture or replacement texture is indicative of a gradual replacement of the serpentine polimorph by carbonate minerals; the relict mesh texture in the serpentinites (Figure 4b) suggests that these rocks originated as Lz-serpentinites [44]. The carbonate minerals are also present in the veins together with talc (Figure 4c) and rare fibrous tremolite (Figure 4d). In some cases, quartz grains show undulous extinction, which suggests dynamic recrystallization (Figure 4e). Furthermore, talc is often associated with serpentine (Figure 4f). Furthermore, clinopyroxene was also detected as a minor phase.

4.2. µ-Raman Spectroscopy

µ-Raman Spectroscopy is particularly useful for quick and reliable identification of carbonate, quartz, talc, serpentine polymorphs, as well as amphibole minerals. For each specimen, several µ-Raman spectra were obtained.

The various serpentine polymorphs (i.e., lizardite, antigorite, chrysotile, and polygonal serpentine) have been characterized. Raman spectra can be observed, all low and high wavenumber, in Figures 5 and 6, respectively. In both fibrous chrysotile and antigorite serpentine polymorphs, the main peaks detected in the Raman spectrum at low wavenumber are associated with the symmetric Si-Ob-Si stretching and SiO_4 bending modes, which occur at 694 and 388 cm^{-1} in chrysotile (Figure 5a) and 687 and 378 cm^{-1} in antigorite (Figure 5b), respectively. Two large peaks, at 235 cm^{-1} in chrysotile and 230 cm^{-1} in antigorite, respectively, are likely related to the O-H-O vibrational modes due to the hydrogen weak bonds. Moreover, based on the 1045 cm^{-1} antisymmetric Si-Ob-Si stretching mode, antigorite was easily distinguished from chrysotile. In the spectral region associated with vibrational modes of the OH groups, antigorite and chrysotile are characterized by very different µ-Raman spectra. Chrysotile exhibits an antisymmetric band at about 3699 cm^{-1}, with a tail toward lower wavenumbers, and a less pronounced peak at about 3691 cm^{-1} (Figure 6a), whereas antigorite shows two main bands at 3701 and 3672 cm^{-1} (Figure 6b).

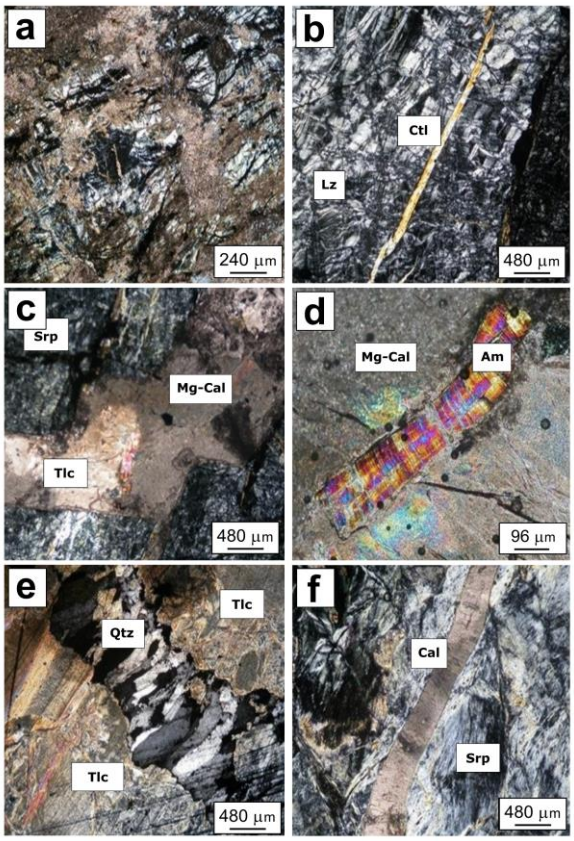

Figure 4. (**a**) Fibrous chrysotile occurs in the serpentine matrix, 2X, NX; (**b**) irregular patchy texture, 4X; (**c**) carbonate veins with talc, 2X, 1X; (**d**) fibrous tremolite in carbonate veins, 10X, cro; (**e**) Quartz vein with undulous extinction and elongate sub-grains, 2X; (**f**) carbonate veins in serpentinites with talc, 2X, 1X. All photomicrographs are at crossed Nicols polarizing conditions. Mineral symbols: srp: serpentinite; cal: calcite; Mg-cal: magnesium-rich calcite; am: amphibole; qtz: quartz; lz: lizardite; ctl: chrysotile; tlc: talc.

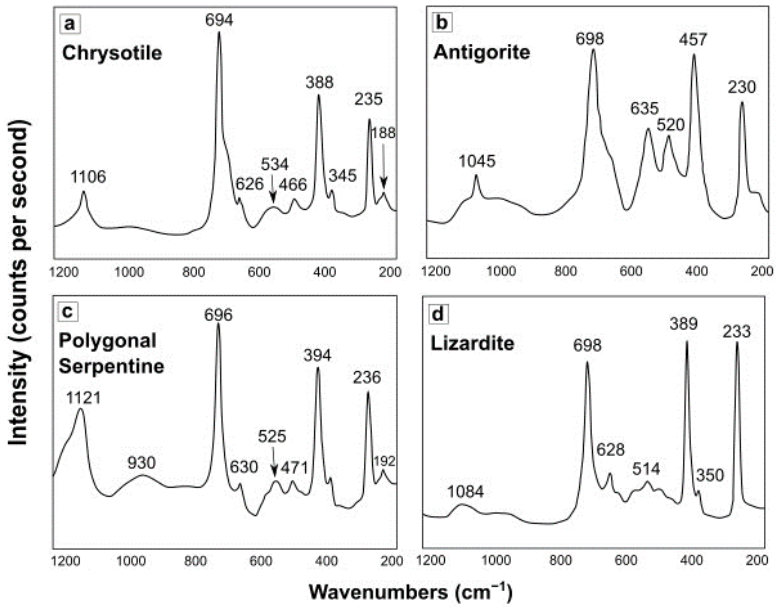

Figure 5. Raman spectra at low wavenumbers of serpentine polymorphs from selected samples. (**a**) chrysotile pattern; (**b**) antigorite pattern; (**c**) Polygonal serpentine pattern; (**d**) lizardite pattern.

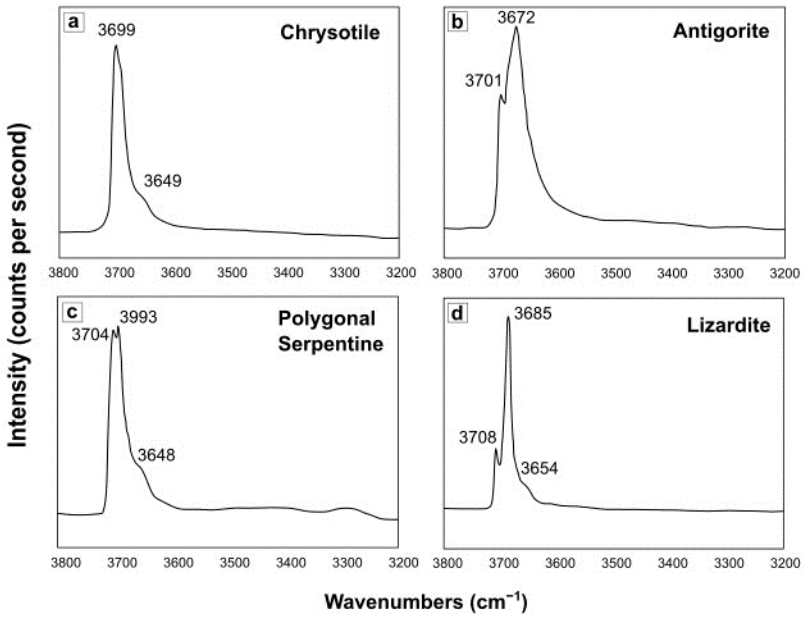

Figure 6. Raman spectra at high wavenumbers of serpentine polymorphs from selected samples. (**a**) chrysotile pattern; (**b**) antigorite pattern; (**c**) Polygonal serpentine pattern; (**d**) lizardite pattern.

Furthermore, light green colored serpentine was identified as polygonal serpentine. This polymorph shows quite similar Raman spectrum to those of the chrysotile either at low or high wavenumbers. The polygonal serpentine, at high wavenumbers, shows large peak consisting of two bands at 3704 and 3693 cm^{-1} with a hump at 3648 cm^{-1} (Figure 6c), whereas chrysotile exhibits a narrow peak composed of 3699 and 3691 cm^{-1} bands with a hump at 3649 cm^{-1}. Lizardite shows a peak at 3708 cm^{-1} and 3685 cm^{-1} (Figure 6d) in the spectral area associated with vibrational modes of the OH groups.

4.3. XRPD Assessment

The X-ray powder diffraction investigation of powdered bulk rock allowed the detection of carbonate minerals, serpentine, and amphibole, which are the principal mineral phases, followed by 2:1 phyllosilicate (Figure 7).

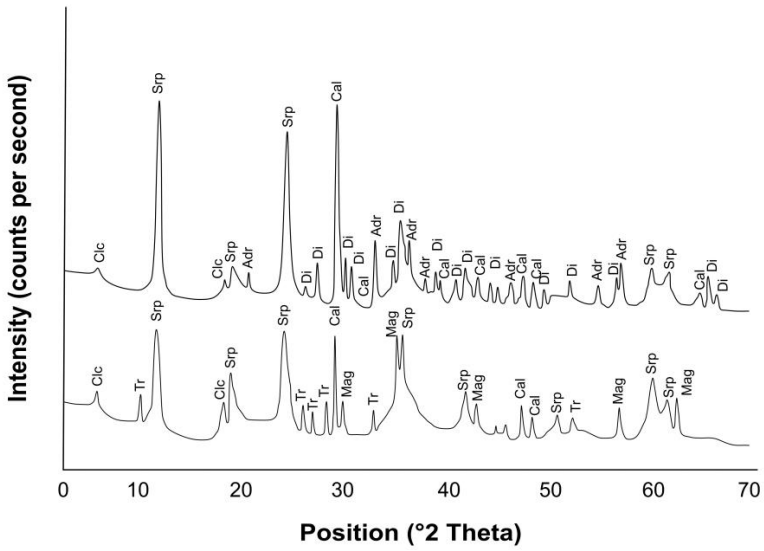

Figure 7. XRPD patterns of selected bulk serpentinites samples from Pietrapica quarry site. Srp = serpentine; Tr = tremolite; Clc = Clinochlore; Adr = Andradite; Di = diopside; Cal = calcite; Mag = magnetite.

4.4. Mineral Chemistry

In selected serpentinite specimens of the Pietrapica quarry, electron probe microanalyses were carried out on different types of minerals, including serpentine, amphibole, chlorite, clinopyroxene, magnetite, talc, quartz and titanite, which are often associated with carbonate veins (Figure 8). The results of electron probe microanalyses are reported in Table 1.

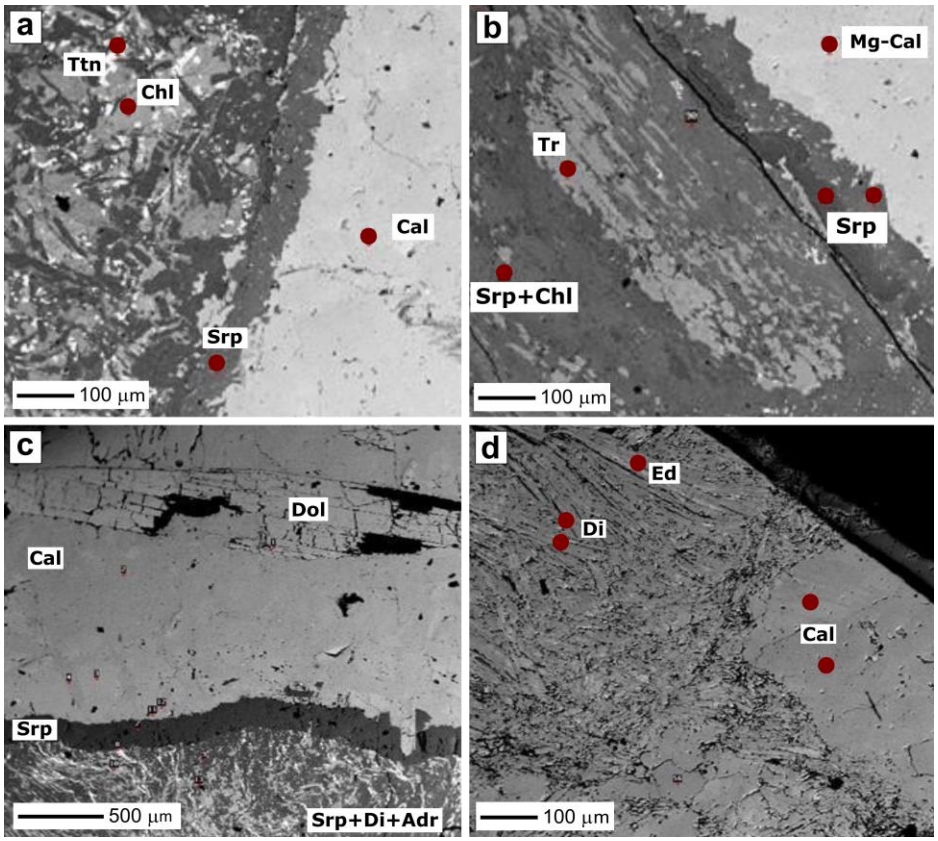

Figure 8. (**a**) serpentine with chlorite and small crystals of titanite infiltrated in calcite matrix; (**b**) fibrous tremolite with serpentine and chlorite; (**c**) contact between carbonate veins and bulk rocks with crenulation cleavage; (**d**) radial-fibrous crystals of diopside with edenite in carbonate veins. Red circles indicate the spot analysis.

Serpentinite-chlorite layers show SiO_2, MgO, Al_2O_3 and FeO median values of 36.21 wt.%, 34.46 wt.% 8.31 wt.% and 5.58 wt.%, respectively. The Ca content (CaO = 0.02–3.48 wt.%) is relatively higher in all the analyzed serpentine.

The chemical compositions of the analyzed amphiboles revealed the occurrence of either Ca-amphiboles or Mg-Fe-Mn amphiboles, showing median values of SiO_2 = 53.73 wt.%, MgO = 23.31 wt.%, Al_2O_3 = 3.17 wt.%, FeO = 2.87 wt.% and CaO = 12.42 wt.%. The calcic amphiboles include edenite, tremolite and Mg-Fe-hornblende.

Cr-spinel EMPA results display high values of Cr_2O_3 (median = 33.87 wt.%), FeO (median = 20.085 wt.%) and Al_2O_3 (median = 16.36 wt.%) with lower abundances of MgO (median = 9.65 wt.%), SiO_2 (median = 1.30 wt.%) and MnO (median = 2.49 wt.%).

Clinopyroxene was analyzed in the matrix as fine-grained and in the carbonate veins as radial-fibrous and euhedral crystals. Results revealed that clinopyroxene is characterized by homogeneous compositions rich in the diopside end-member, with high SiO_2 (median = 53.63 wt.%), MgO (median = 16.99 wt.%) and CaO (median = 24.77 wt.%) contents.

Table 1. EMPA results (major oxides) on different minerals found in the Pietrapica serpentinites. n.d. = not detected.

Spot Analysis	SiO_2	MgO	Al_2O_3	FeO	TiO_2	Cr_2O_3	MnO	CaO	Na_2O	P_2O_5	NiO	Total
serpentine-chlorite mixed layers												
1	38.850	35.65	4.48	5.28	0.032	n.d.	0.1	0.088	n.d.	n.d.	0.16	84.64
2	39.30	36.36	4.46	5.2	0.001	0.002	0.12	0.023	n.d.	0.018	0.21	85.69
3	37.180	34.46	6.90	4.96	n.d.	0.384	0.15	0.226	0.002	0.015	0.22	84.49
4	36.820	35.67	6.10	5.02	0.03	0.013	0.1	0.054	n.d.	n.d.	n.d.	83.8
5	41.210	36.9	1.70	4.59	0.039	0.061	0.06	0.155	n.d.	0.004	0.02	84.74
6	38.80	36.31	4.20	4.76	n.d.	0.031	0.08	0.039	0.006	0.001	0.06	84.29
7	39.260	36.39	4.40	4.83	n.d.	0.017	0.13	0.005	0.048	0.05	0.07	85.2
8	36.090	35.15	7.51	5.36	n.d.	0.059	0.03	0.003	n.d.	0.015	0.08	84.29
9	39.240	36.24	4.14	5.26	0.003	n.d.	0.12	0.077	0.037	n.d.	0.06	85.18
10	39.180	36.12	4.25	4.86	0.018	n.d.	0.07	0.071	n.d.	n.d.	0.03	84.6
11	39.470	34.99	4.61	4.98	0.036	0.222	0.06	1.270	0.011	n.d.	0.19	85.84
12	36.120	34.32	8.59	5.96	0.022	0.055	0.09	0.033	0.003	n.d.	0.11	85.3
13	38.160	33.31	6.49	4.94	0.47	0.345	0.04	0.819	0.022	0.014	0.02	84.63
14	39.340	33.07	5.36	5.28	0.161	0.238	0.08	2.10	0.02	n.d.	0.04	85.68
15	40.020	33.78	5.44	4.84	0.04	0.228	0.12	0.464	n.d.	n.d.	n.d.	84.93
16	38.210	32.91	7.98	4.71	0.032	0.376	0.12	1.210	0.009	0.025	n.d.	52.67
17	39.370	35.2	4.76	5.33	n.d.	0.07	0.13	0.071	n.d.	0.015	0.04	84.99
18	37.170	35.26	7.01	5.02	0.002	n.d.	0.06	0.033	n.d.	n.d.	0.03	84.59
19	39.510	35.38	5.93	5.03	0.004	0.015	0.09	0.062	n.d.	n.d.	n.d.	86.02
20	39.470	32.42	4.86	5.69	0.317	0.221	0.11	3.480	0.011	0.021	0.07	86.68
21	38.220	34.73	5.98	5.39	0.06	0.032	0.04	0.218	0.032	n.d.	0.1	84.8
22	38.730	35.77	5.69	5.64	0.002	0.038	0.03	0.115	n.d.	0.01	0.1	86.12
23	37.390	35.59	6.93	5.15	0.007	0.019	0.12	0.043	0.003	n.d.	0.06	85.31
24	38.880	34.03	5.15	6.09	0.165	0.059	0.13	1.220	0.021	n.d.	0.02	85.76
25	39.140	33.27	6.67	4.77	n.d.	0.317	0.09	1.880	0.005	0.015	0.03	86.19
26	37.780	36.06	5.83	5.29	n.d.	0.001	0.09	0.035	0.036	0.012	0.19	85.33
27	38.650	35.22	4.02	6.02	0.042	n.d.	0.05	0.17	0.03	0.022	0.18	84.4
28	37.850	34.48	6.28	5.49	0.019	0.026	0.1	0.104	0.098	n.d.	0.16	84.61
29	37.250	35.27	5.87	5.14	n.d.	n.d.	0.05	0.038	0.082	n.d.	0.16	83.86
30	37.560	35.53	6.01	5.26	0.004	0.005	0.09	0.048	0.004	0.07	0.07	84.65
31	38.060	36.48	5.41	4.97	0.003	n.d.	0.06	0.022	0.011	n.d.	0.21	85.22
32	34.080	33.26	10.98	7.19	0.002	0.014	0.06	0.116	n.d.	0.022	0.08	85.8
33	36.910	34.14	9.15	4.98	0.031	0.063	0.04	0.126	n.d.	0.024	0.04	85.5
34	37.010	35.54	8.16	6.12	0.034	n.d.	0.07	0.097	0.016	0.01	0.14	87.2
35	34.210	33.74	10.65	7.68	n.d.	n.d.	0.11	0.116	n.d.	n.d.	0.05	86.56
36	40.990	38.04	3.97	6.43	0.006	n.d.	0.06	0.165	n.d.	n.d.	0.1	89.76
37	39.640	36.03	5.11	6.46	0.12	0.036	0.16	0.161	0.084	0.028	0.08	87.9
38	37.960	34.89	7.66	5.47	0.022	0.059	0.12	0.127	0.015	0.022	0.09	86.43
39	37.130	35.49	8.31	4.14	0.152	n.d.	0.04	0.157	n.d.	0.009	0.09	85.52
40	35.860	34.04	10.36	6.62	0.018	0.022	0.01	0.103	0.032	0.013	0.01	87.09
41	35.220	33.25	10.75	6.81	0.037	0.074	0.06	0.108	n.d.	n.d.	0.01	86.32
42	35.690	34.84	9.5	5.22	0.015	n.d.	0.05	0.074	0.015	0.029	0.01	85.45
43	35.480	33.96	9.81	7.4	0.009	0.012	0.09	0.111	n.d.	0.004	0.12	86.99
44	36.620	35.22	10.19	5.3	0.018	0.005	0.1	0.073	0.028	0.023	0.01	87.59
45	36.180	34.39	9.27	6.34	0.02	0.03	0.16	0.077	n.d.	0.012	0.06	86.54
46	35.990	33.89	9.42	6.35	0.02	0.067	0.09	0.1	0.024	0.026	0.09	86.06
47	36.450	35.42	8.43	6.3	0.029	0.048	0.1	0.098	0.013	0.004	n.d.	86.89
48	36.940	33.94	9.23	6.54	0.025	0.043	n.d.	0.247	0.022	0.011	0.11	87.11
49	43.40	38.68	1.97	6.05	0.007	0.042	0.05	0.209	n.d.	0.016	0.09	90.51
50	36.210	34.47	9.36	5.85	n.d.	n.d.	0.08	0.088	0.029	n.d.	0.05	86.13
51	36.60	35.17	9.19	5.58	n.d.	0.027	0.08	0.049	n.d.	n.d.	0.08	86.78
52	34.580	34.08	10.28	7.51	n.d.	n.d.	0.03	0.118	0.001	n.d.	0.08	86.68
53	34.80	33.94	9.61	8.08	0.047	n.d.	0.02	0.107	0.001	n.d.	0.05	86.65
54	44.360	38.55	1.55	6.05	n.d.	n.d.	0.07	0.257	0.015	n.d.	0.14	90.99
55	35.690	34.84	9.5	5.22	0.015	n.d.	0.05	0.074	0.015	0.041	0.05	85.5
56	35.480	33.96	9.81	7.4	0.009	0.012	0.09	0.111	n.d.	n.d.	n.d.	86.87
57	36.340	35.22	10.19	5.3	0.018	0.005	0.1	0.073	0.028	n.d.	n.d.	87.28
58	36.180	34.39	9.27	6.34	0.02	0.03	0.16	0.077	n.d.	0.066	0.06	86.58
59	35.990	33.89	9.42	6.35	0.02	0.067	0.09	0.1	0.024	n.d.	0.1	86.04
60	36.450	35.42	8.43	6.3	0.029	0.048	0.1	0.098	0.013	0.025	0.1	87.02
61	35.940	33.94	9.28	6.56	0.025	0.043	n.d.	0.247	0.022	0.018	0.07	86.14
62	43.40	38.68	1.97	6.05	0.007	0.042	0.05	0.209	n.d.	0.032	0.08	90.51

Table 1. *Cont.*

Spot Analysis	SiO_2	MgO	Al_2O_3	FeO	TiO_2	Cr_2O_3	MnO	CaO	Na_2O	P_2O_5	NiO	Total
63	36.210	34.47	9.36	5.58	n.d.	n.d.	0.08	0.088	0.029	n.d.	0.08	85.9
64	36.60	35.17	9.19	5.58	n.d.	0.027	0.08	0.049	n.d.	n.d.	0.11	86.8
65	34.580	34.07	10.28	7.51	n.d.	n.d.	0.03	0.118	0.001	0.017	0.11	86.72
66	34.80	33.94	9.61	8.08	0.047	n.d.	0.02	0.107	0.001	n.d.	0.04	86.65
67	44.360	38.55	1.55	6.05	n.d.	n.d.	0.07	0.257	0.015	0.015	0.07	90.93
68	33.420	32.59	11.91	7.14	0.059	0.493	0.02	0.276	n.d.	0.009	0.06	85.97
69	33.580	32.82	12.57	6.82	0.023	0.066	0.14	0.047	0.031	0.026	0.03	86.16
70	32.430	30.03	15.49	8.03	n.d.	0.049	0.16	0.04	n.d.	0.04	0.07	86.33
71	35.750	32.57	9.59	6.51	1.530	0.086	0.17	1.290	0.002	n.d.	0.08	87.58
72	36.630	33.89	1.13	6.24	0.011	0.027	0.02	0.154	n.d.	0.01	0.09	78.2
73	34.850	32.78	9.98	7.69	n.d.	n.d.	0.05	0.597	n.d.	0.031	0.06	86.04
74	37.120	34.37	8.4	5.43	0.052	0.038	0.02	0.067	0.026	n.d.	0.05	85.56
75	33.440	31.61	12.69	7.53	0.001	n.d.	0.02	0.109	0.018	n.d.	0.06	85.47
76	34.90	34.66	9.5	6.91	0.008	0.031	0.09	0.176	0.009	0.01	0.02	86.31
77	36.920	35.21	8.66	5.85	0.029	0.077	0.11	0.094	0.003	0.016	0.04	87.02
78	35.0	32.07	11.73	6.87	0.012	0.145	0.16	0.685	0.018	0.028	0.02	86.74
79	40.290	37.61	3.39	5.97	0.026	n.d.	0.06	0.145	0.018	n.d.	0.04	87.55
80	36.470	36.81	9.04	4.77	0.006	0.024	0.05	0.124	0.016	0.005	0.01	87.33
81	36.610	35.43	8.68	4.94	0.046	n.d.	0.05	0.079	0.016	0.024	0.05	85.92
					Anphiboles							
1	44.26	24.92	4.25	4.33	0.241	0.204	0.1	11.63	0.057	0.014	0.12	90.12
2	40.68	12.91	1.04	1.9	n.d.	0.022	0.07	31.78	0.082	0.017	0.01	88.52
3	40.97	23.13	8.41	2.61	0.016	0.029	0.09	13.05	0.21	0.026	0.06	88.6
4	43.81	28.9	3.58	3.86	0.018	0.137	0.08	8.72	0.033	0.005	0.09	89.23
5	47.59	14.72	10.81	1.18	0.017	0.01	0.1	21.81	0.149	0.009	n.d.	96.4
6	54.58	23.1	2.79	3.92	0.158	0.224	0.14	11.42	1	0.02	0.11	97.65
7	57.39	23.41	0.47	3.14	0.011	0.007	0.09	13.57	0.09	n.d.	0.09	98.27
8	55.67	24.4	1.55	2.47	0.059	0.092	0.05	12.84	0.459	0.022	0.05	97.66
9	52.04	22.6	5.28	3.23	0.433	0.425	0.03	11.95	1.18	0.057	0.08	97.3
10	53.73	23.23	3.54	3.06	0.268	0.486	0.12	12.06	1.14	0.013	0.08	97.72
11	57.54	23.52	1.36	2.66	0.075	0.009	0.08	12.27	0.358	0.017	0.05	97.94
12	51.65	21.81	5.48	2.87	0.482	0.502	0.03	12.42	1.29	0.014	0.14	96.69
13	55.26	20.99	1.87	7.06	0.065	0.006	0.17	9.68	1.99	0.012	0.05	97.15
14	55.01	23.62	2.5	2.4	0.059	0.225	0.08	12.52	0.813	0.023	n.d.	97.25
15	57.33	23.44	n.d.	2.01	n.d.	n.d.	0.02	13.65	0.07	0.013	n.d.	96.54
					Cr-Spinel							0
1	0.03	14.06	30.53	15.59	0.12	36.39	0.08	n.d.	0.01	0.009	0.03	96.851
2	2.57	2.75	1.56	25.77	0.43	28.98	5.13	0.05	0.02	0.026	0.05	67.340
3	0.03	14.69	29.68	14.47	0.11	37.27	0.1	n.d.	n.d.	0.04	0.03	96.417
4	3.28	3.59	2.24	25.25	0.47	32.3	5.41	0.06	0.04	n.d.	0.05	72.685
5	4.34	5.35	3.04	24.66	0.46	29.86	4.88	0.09	0.05	0.01	0.02	72.759
6	0.03	13.96	30.4	15.69	0.13	35.96	0.11	0.02	n.d.	0.031	0.06	96.387
7	0.03	14.08	31.39	15.81	0.13	35.52	0.06	0.01	n.d.	n.d.	0.06	97.085
8	4.21	4.76	1.85	24.89	0.51	30.77	5.33	0.07	0.07	n.d.	0.05	72.507
9	0.03	13.95	30.89	15.94	0.14	36.03	0.11	0.01	0.01	0.01	0.05	97.167
10	3.83	4.24	1.9	24.23	0.45	29.11	4.91	0.28	0.06	0.016	0.08	69.107
11	0.04	14.2	30.07	15.06	0.14	35.44	0.09	n.d.	n.d.	0.028	0.04	95.111
12	3.98	4.38	1.61	24.92	0.42	29.43	5.03	0.06	0.04	n.d.	0.05	69.920
					Clynopyroxene							0
1	54.47	17.37	0.241	0.880	0.048	n.d.	0.05	26	0.009	0.024	0.02	98.95
2	54.63	17.28	0.456	2.20	0.1	0.052	0.17	24	0.035	0.057	n.d.	99.4
3	52.14	17.06	1.040	3.80	0.111	0.156	0.3	23.57	0.108	n.d.	0.01	98.3
4	54.43	17.76	0.035	1.360	0.045	0.043	0.25	25	n.d.	0.118	n.d.	99.48
5	53.35	17.68	0.958	1.250	0.006	0.015	0.15	23.64	0.102	n.d.	0.01	97.17
6	54.45	17.10	0.259	1.30	0.006	n.d.	0.06	25.34	0.057	0.001	0.04	98.62
7	52.41	14.990	1.60	1.150	n.d.	0.003	0.12	24	0.051	0.038	0.05	94.88
8	53.06	16.510	1.590	2.30	0.017	0.016	0.18	25	0.145	0.022	n.d.	98.36
9	53.45	16.910	0.858	1.760	0.025	n.d.	0.08	25	0.091	0.065	0.05	98.12
10	53.37	17.50	0.747	1.340	n.d.	0.024	0.04	25	0.071	0.028	0.06	97.89
11	49.36	16.880	1.750	1.660	0.003	n.d.	0.09	24	0.113	0.032	0.02	93.96
12	54.12	16.72	0.486	1.850	0.012	0.013	0.12	25	0.076	0.015	n.d.	98.64
13	52.95	16.70	0.785	1.960	0.012	0.006	0.12	24.940	0.062	0.037	0.05	97.62
14	54.29	17.10	0.382	1.430	0.021	0.003	0.14	26	0.102	0.032	0.03	99.02
15	53.87	16.99	0.388	2.850	0.023	0.007	0.12	25	0.056	0.062	0.01	99.78
16	54.59	17.980	0.027	1.060	n.d.	n.d.	0.1	26	n.d.	0.018	0.02	99.48
17	53.32	17.060	0.56	2.10	0.052	n.d.	0.31	24	0.055	0.025	n.d.	97.8
18	53.82	16.660	0.143	1.940	0.033	0.01	0.28	26	n.d.	0.032	n.d.	98.59

Table 1. *Cont.*

Spot Analysis	SiO_2	MgO	Al_2O_3	FeO	TiO_2	Cr_2O_3	MnO	CaO	Na_2O	P_2O_5	NiO	Total
					Talc							0
1	59.4	29.65	0.52	2.65	0.024	0.006	n.d.	0.177	0.033	n.d.	0.14	92.6
2	59.26	29.76	0.556	2.63	0.05	n.d.	0.02	0.164	0.059	n.d.	0.08	92.58
3	60.01	28.93	0.537	2.56	0.009	0.005	n.d.	0.22	0.039	0.025	0.13	92.47
4	59.58	30.09	0.653	3.78	n.d.	n.d.	0.03	0.262	0.077	n.d.	0.07	94.54
5	60.24	29.69	0.487	2.41	0.019	n.d.	n.d.	0.138	0.055	n.d.	0.12	93.16
6	59.45	28.78	0.637	2.53	n.d.	n.d.	0.01	0.161	0.098	0.008	0.07	91.74
7	60.63	28.99	0.573	2.72	0.012	n.d.	n.d.	0.159	0.066	n.d.	0.11	93.26
8	59.86	28.17	0.65	2.5	n.d.	0.01	n.d.	0.204	0.363	0.018	0.03	91.8
9	60.42	27.97	0.42	2.53	0.012	0.02	n.d.	0.166	0.088	0.001	0.06	91.69
10	60.53	29.2	0.265	3.3	n.d.	0.01	n.d.	0.12	0.076	0.006	0.05	93.56
11	59.61	30.28	0.581	2.77	n.d.	n.d.	0.05	0.159	0.082	0.023	0.06	93.61
12	59.14	29.56	0.566	2.63	n.d.	0.023	0.04	0.224	0.053	0.007	0.11	92.35
13	58.18	28.48	0.35	2.22	0.035	0.014	0.02	0.106	0.061	0.003	0.15	89.62
14	58.26	27.26	0.539	2.82	0.007	0.081	n.d.	0.175	0.031	0.036	0.01	89.22
15	58.58	29.34	0.601	3.45	0.034	n.d.	0.01	0.227	0.101	0.027	0.1	92.47
16	60.33	28.83	0.651	2.83	n.d.	n.d.	n.d.	0.207	0.052	0.001	0.11	93.01
17	61.63	27.81	0.377	2.75	0.008	n.d.	n.d.	0.078	0.101	0.004	0.07	92.83
18	59.22	29.89	0.337	2.77	0.002	n.d.	n.d.	0.173	0.042	0.039	0.1	92.57
19	60.62	29.82	0.255	3.34	0.013	0.032	0.01	0.111	0.037	n.d.	0.16	94.4
20	58.79	27.33	0.42	3.37	n.d.	n.d.	0.03	0.232	0.041	0.004	0.11	90.33
21	60.63	28.47	0.524	2.89	0.027	n.d.	n.d.	0.105	0.034	n.d.	n.d.	92.68
22	61.43	28.58	0.554	2.93	n.d.	n.d.	n.d.	0.114	0.064	0.01	0.1	93.79
23	60.43	29.43	0.39	2.66	n.d.	n.d.	0.02	0.127	0.058	n.d.	0.06	93.17
					Titanite and magnetite							0
1	1.70	1.20	0.79	80.71	n.d.	0.217	0.07	0.185	0.016	0.047	0.02	84.96
2	0.616	0.324	0.13	84.14	0.066	0.141	0.04	0.231	n.d.	0.053	0.03	85.78
3	0.759	0.492	0.59	77.23	0.138	7.1	0.47	0.086	0.091	0.165	0.04	87.16
4	0.874	0.428	4	80.8	0.124	0.303	0.06	0.534	0.077	0.053	0.07	87.79

The EMPA results related to talc show high abundances of SiO_2 (median = 56.61 wt.%), MgO (median = 28.939 wt.%) and less content of FeO (median = 2.75 wt.%) while titanite-magnetite composition is dominated by FeO (median = 72.02 wt.%) and Al_2O_3 content (median = 53.63 wt.%).

Titanite and magnetite minerals show that they are mainly composed of FeO (median = 80.75 wt.%).

4.5. Bulk Geochemistry: Major and Trace Elements

The whole rock chemical composition of the serpentinite samples is shown in Table 2.

Major elements composition is dominated by SiO_2 (median = 42.06 wt.%; st.dev = 0.55) and MgO (median = 41.87 wt.%; st.dev = 0.74) with less presence of Fe_2O_3 (median = 13.19 wt.% st.dev = 0.32) and Al_2O_3 (median = 1.6 wt.% st.dev = 0.41) (Figure 9). The most abundant trace elements are Ni (median = 2313 ppm; st.dev = 88.22) and Cr (median = 3234; ppm st.dev = 906.54) while the rest of trace elements such as V (median = 72 ppm; st.dev = 23.74), Co (median = 112.34 ppm; st.dev = 5.61), Cu (median = 15.86 ppm; st.dev = 0.37), Zn (median = 44.05 ppm; st.dev = 6.48), Ba (median = 52.5 ppm; st.dev = 27.70), Sr (median = 18 ppm; st.dev = 12.08), Zr (median = 24.5 ppm; st.dev = 2.32), S (median = 186 ppm; st.dev = 52.21), Cl (median = 202; ppm st.dev = 47.75) display quite minor concentrations. As shown in Figures 9 and 10, the chemical elements that show higher content dispersion are Al_2O_3, TiO_2 and CaO for major oxides and V, Ba, S and Cl for the trace elements.

Table 2. Bulk chemical composition of the studied serpentinite samples. d.l. = detection limit.

	d.l.	PP1	PP2	PP3	PP4	PP5	PP6
%							
SiO_2	0.01	41.8	41.54	41.12	42.38	42.53	42.32
TiO_2	0.001	0.18	0.1	0.22	0.08	0.13	0.09
Al_2O_3	0.001	2.11	1.4	1.22	1.95	1.09	1.8
Fe_2O_3(T)	0.01	13.24	13.45	13.59	13.1	12.65	13.14
MnO	0.001	0.11	0.12	0.12	0.13	0.11	0.12
MgO	0.01	40.9	42.8	42.14	40.9	41.73	42.01
CaO	0.01	1.52	0.3	1.28	0.79	1.24	0.06
K_2O	0.01	0.01	0.01	0.02	0.01	0.02	0.01
Total		99.87	99.54	99.71	99.34	99.5	99.55
LOI		11.21	11.38	11.55	10.89	11.12	10.97
ppm							
Ni	20	2220.54	2440.53	2312.42	2297.15	2313.03	2445.98
Cr	20	2890	3104	5355	3687	3284	3184
V	5	98	45	56	100	58	86
Co	1	112.86	113.68	107.64	114.19	111.82	99.54
Cu	10	15.79	15.2	16.12	15.94	16.25	15.79
Zn	30	43.76	54.2	35.77	44.34	44.85	37.76
Ba	5	30	75	24	81	77	28
Sr	2	46	19	18	14	15	18
Zr	4	24	27	25	28	23	22
S	5	125	220	232	155	217	114
Cl	5	184	245	290	187	159	217

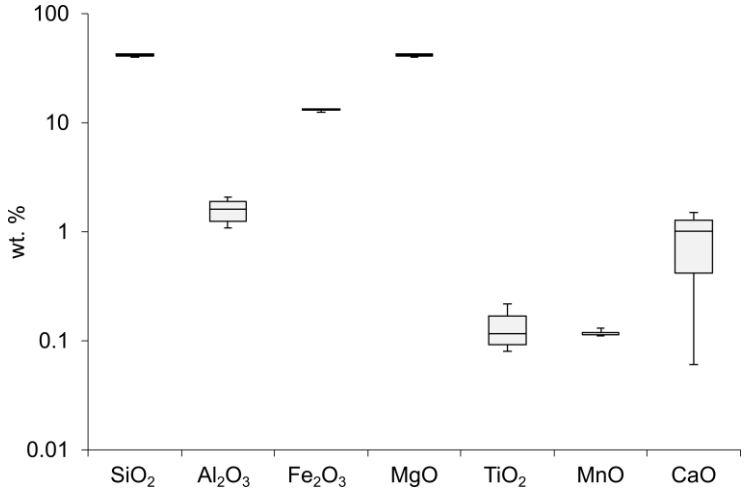

Figure 9. Box and whiskers plot for major elements oxides in studied samples.

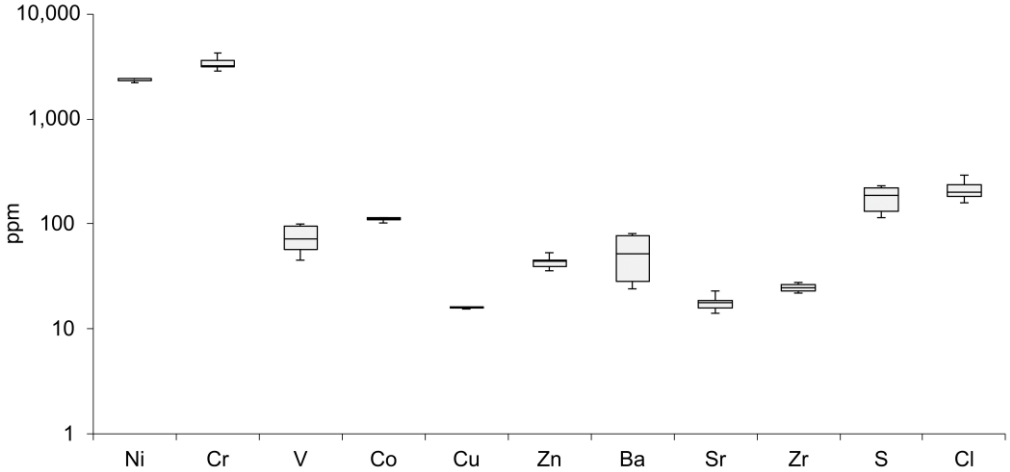

Figure 10. Box and whiskers plot for trace elements in the studied samples.

Comparing the chemical composition of the Pietrapica serpentinites with those cropping out in abandoned quarries in Calabria (Gimigliano and Mt Reventino [23,24], we observed very similar abundances regarding the main major oxides SiO_2 (Pietrapica 41.12–42.53 wt.%, median = 42.06 wt.%; Gimigliano 37.36–40.81 wt.%, median = 40.04 wt.%; Reventino Mt. 38.70–40.78 wt.%, median = 39.73 wt.%) and MgO (Pietrapica 40.90–42.80 wt.%, median = 41.87 wt.%; Gimigliano 36.61–39.09 wt.%, median = 37.08 wt.%; Reventino Mt. 36.94–39.48 wt.%, median = 39.10 wt.%) while the Fe_2O_3 values in Pietrapica serpentinite is slightly higher (Pietrapica 12.65–13.59 wt.% median = 13.19 wt.%; Gimigliano 6.98–8.13 wt.%, median = 7.30 wt.%; Reventino Mt. 6.76–8.40 wt.%, median = 6.95 wt.%) (Figure 11).

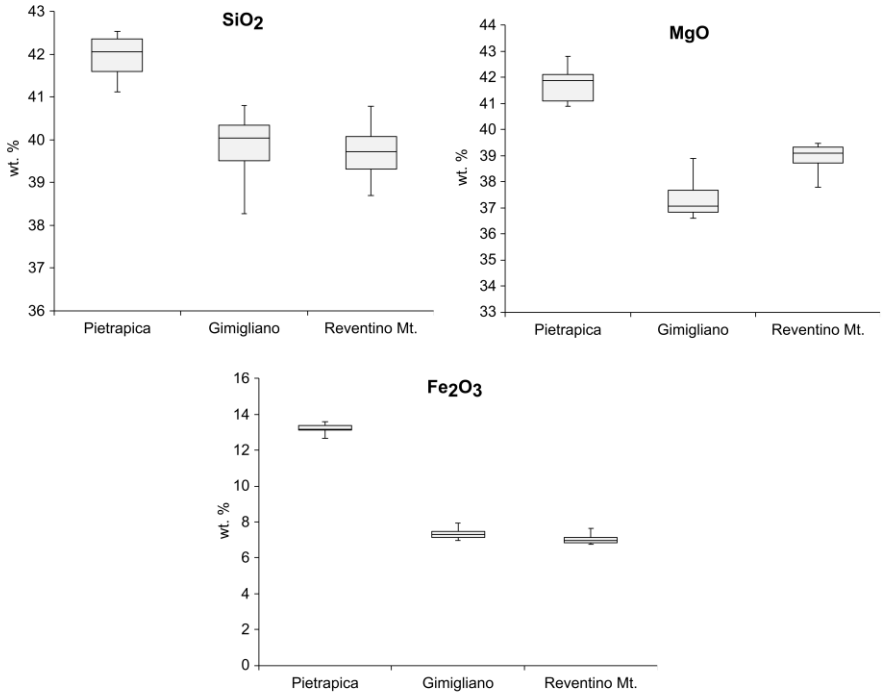

Figure 11. Box and whiskers plot for major oxides in the Pietrapica, Gimigliano and Reventino Mt. serpentinites.

Regarding the most enriched trace elements, it has been observed that Pietrapica serpentinites are richer in the most abundant trace elements Ni (2220.54–2445.98 ppm, median = 2312.73 ppm) and Cr (2890–5355 ppm, median = 3234 ppm) with respect the Gimigliano (Ni 1217.51–2050.84 median = 1688.60 ppm; Cr 1525.40–2904.75, median = 2226.63 ppm) and Mt Reventino serpentinites (Ni 1829–2241 ppm, median = 1937.22 ppm; Cr 1772.62–3524.12 ppm, median = 2606.64 ppm) samples (Figure 12).

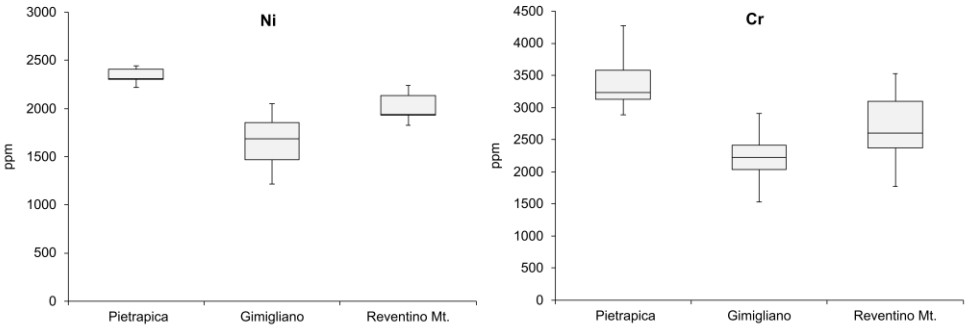

Figure 12. Box and whiskers plot for trace elements in the Pietrapica, Gimigliano and Reventino Mt. serpentinites.

5. Discussion and Conclusions

The microstructural and petrographical features of the studied serpentinites revealed that they are the result of the serpentinization of mantle peridotites (lherzolite and subordinately harzburgite) equilibrated under the spinel-peridotite facies [39].

Despite being widely used and marketed as dimension stone, serpentinite rocks may go through various modifications after their "switch in service" from natural occurrences (i.e., ophiolite outcrops) to building and construction materials. A detailed characterization under the petrographic, mineralogical and geochemical points of view permits, on the one hand, to avoid and prevent unexpected behavior of serpentinites used as building stones; on the other hand, it provides a useful tool from an univocal identification of serpentinite employed in the monuments, in term of provenance [12,13]. This is also a prominent point for the serpentinite rocks that crop out in the Basilicata region since they were exploited and marketed up to the recent past as dimension stones; indeed, they may still constitute an important resource, provided that their characterization is strictly essential and must forerun their use as construction and/or conservation–restoration material, in the frame of architectonic and cultural heritage.

Moreover, it is noteworthy that it has been observed that the weathering of the rocks that constitute the ophiolite outcrops can represent a potential source of toxic elements, in particular the first-row transition elements such as Cr and Ni contents, whose contents within the serpentinite outcrops in the northern sector of the Pollino massif are largely higher than those ones ascribed to the upper continental crust [45,46]. Generally, the weathering of serpentinite rocks is associated with Mg-HCO_3 type water types, which are slightly alkaline (e.g., [47–49]). In addition to serpentinite, in the study area, geological surveys pointed out that another source of potentially toxic elements may derive from the weathering of intermediate to lower crustal rocks because, compared to the average upper continental crust, they are enriched in elements such as Ni and Cr [45]. According to the literature, nickel is mobile in sulfur-poor systems as Ni^{2+}, especially under climatic and morphological conditions that do not promote either the development of an evolved weathering cover or the occurrence of Fe-hydroxides capable of adsorbing Ni. As far as Cr, it has been seen that chromite dissolution, together with the disintegration of chromite exsolution rims with minor contributions of Cr after magnetite dissolution, are the main geochemical processes responsible for Cr release in the environment [50]. According to the literature [51–53], Cr(III) is considered to induce relatively low toxicity since it is relatively insoluble and immobile at neutral at alkaline-type pH conditions; on the contrary, Cr(VI), which is assessed as an environmental toxin and human carcinogen element: is highly soluble and mobile at neutral at alkaline pH conditions. Moreover, it has been reported that chromium (III) can be readily oxidized to chromium (VI) by naturally occurring Mn(III, IV) oxides (e.g., [54–57]), whereas Cr(VI) can be reduced by organic carbon, sulfide, and Fe(II) (e.g., [58,59]).

In this context, our results deriving from bulk chemistry investigation showed that Cr and Ni are the most abundant heavy metals detected in the studied serpentinite rocks. Even if no limit of toxic element values has been currently established for rocks and minerals, as a reference, we applied to the investigated serpentinite the same thresholds that have been established by the Italian government [60] as limit values for soil and stream water. This may be a useful tool for assessing the potential hazard consequent to the high values of some heavy metals in some "sentinel" rocks, such as serpentinite. Results revealed that Cr and Ni are beyond the maximum permissible contents (Figure 13), which have been established by Italian law for public, private, and residential green use (Limit A, Cr = 150 ppm; Ni = 120 ppm) and commercial and industrial use (Limit B, Cr = 800 ppm; Ni = 500 ppm), respectively.

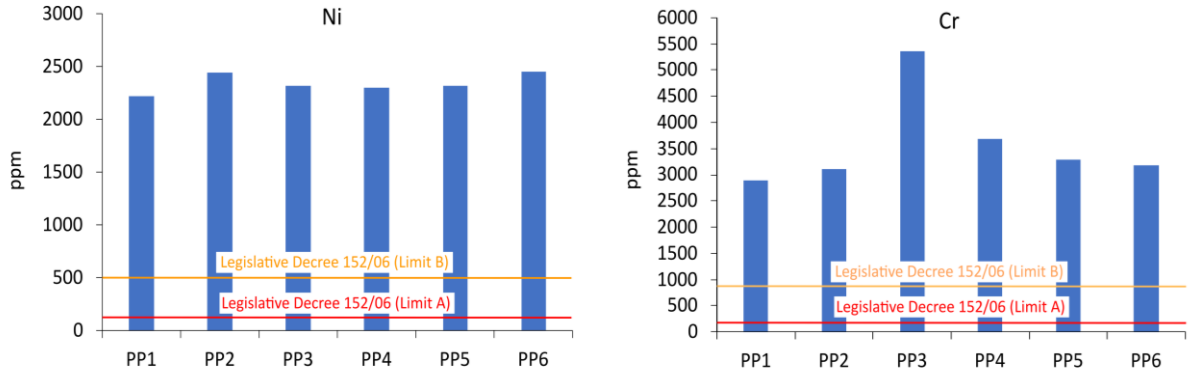

Figure 13. Ni and Cr abundances in studied samples and limit values of Legislative Decree Limit A and Limit B.

As previously stated, it is worth noting that heavy metals such as chromium and nickel are particularly abundant in the ultramafic rocks and ophiolites as well as in some crystalline rocks; moreover, soils resulting from the pedogenetic processes that took place on these lithotypes inherited this heavy-metal enriched fingerprint [61]. The weathering of such rocks can also determine the release in the circulating waters of high amounts of such metals in ionic form. In this regard, the Pollino massif, where the Pietrapica quarry is located, is characterized by the presence of ophiolite and crystalline rocks of continental origin, which are natural reservoirs of chromium and nickel. Even though the content reported in the present study refers to total Cr amount, without any distinction among Cr (VI), which is included in group 1 of carcinogenic substances by WHO, and Cr (III), which is classified within group 3 by WHO, studies carried out in the same area reported similar high contents and suggest that exposure to trivalent chromium can lead to DNA damage detectable in human lymphocytes and that the absorption of Cr (III) in the exposed population may be slow but effective provided that the exposure is continued for prolonged periods (e.g., [57,62]). These data agree with previous ones (e.g., [63–65]). On the other hand, some of these heavy metals have been recently listed by Europe as critical raw materials (e.g., nickel, copper, cobalt), and others assessed at risk of supply (e.g., chromium).

Therefore, abandoned quarries may also be considered in a new light by considering their potentiality assessment.

Finally, since serpentinite rocks are related to asbestos natural occurrences, recognized as carcinogenic to humans [66,67] and reported in other serpentinite outcrops of the Basilicata region (literature), the detailed petrographic, mineralogical and geochemical characterization of serpentinite quarries from Basilicata region can contribute to providing compulsory data as established by Italian law [68] concerning local mapping indicating areas where asbestos and should encourage local, regional and national authorities in planning good practices to prevent asbestos exposure risks.

The detailed knowledge of compositional and microstructural features of historical quarries of serpentinite rocks is fundamental for their characterization, and the study of the evolution and weathering of such rocks in the outcrop can serve as a natural analog for the evolution of a natural rock once placed in a construction site.

Knowledge of the provenance of the serpentinite rocks from which the tiles were made will assure a predicted pattern of their evolution through weathering, avoiding unwanted contrasts in appearance and behavior. Even though this is important in commercial buildings, it should be mandatory in the restoration of monuments. Protecting historical quarries from incorrect exploitation or abandoning has currently become an important issue, also in view of the recent European green strategy recovery of critical raw materials from mining aimed at waste management in an environmentally sound manner.

Author Contributions: Conceptualization, R.P. and G.R.; formal analysis, M.D.; graphics, R.B.; writing—original draft preparation, R.B.; writing—review and editing, G.R. and R.P.; supervision, G.M. All authors have read and agreed to the published version of the manuscript.

Funding: This research was partially funded by University of Catania: (a) (PIAno di inCEntivi per la RIcerca di Ateneo 2020/2022—Pia.Ce.Ri), Grant Number: 22722132153, within the project: "Combined geomatic and petromatic applications: The new frontier of geoscience investigations from field- to micro-scale—(GeoPetroMat)" and (b) PIAno di inCEntivi per la RIcerca di Ateneo 2020/2022 linea 1 Chance grant number 22722132173 P.I., R. Punturo.

Data Availability Statement: The authors did not receive support from any organization for the submitted work.

Conflicts of Interest: The authors declare no conflict of interest.

References

1. Stüwe, K.; Sandiford, M. A description of metamorphic PTt paths with implications for low-P high-T metamorphism. *Phys. Earth Planet. Inter.* **1995**, *3–4*, 211. [CrossRef]
2. Barbieri, M.; Masi, U.; Tolomeo, L. Stable isotope evidence for a marine origin of ophicalcites from the north-central Apennines (Italy). *Mar. Geol.* **1979**, *30*, 193–204. [CrossRef]
3. Lemoine, M. Serpentinites, gabbros and ophicalcites in the Piemont-Ligurian domain of the Western Alps; possible indicators of oceanic fracture zones and of associated serpentinite protrusions in the Jurassic-Cretaceous Tethys. *Arch. Sci.* **1980**, *33*, 103–115.
4. Weissert, H.J.; Bernoulli, D. A transform margin in the Mesozoic Tethys: Evidence from the Swiss Alps. *Geol. Runds.* **1985**, *74*, 665–679. [CrossRef]
5. Früh-Green, G.L.; Weissert, H.; Bernoulli, D. A multiple fluid history recorded in Alpine ophiolites. *J. Geol. Soc.* **1990**, *147*, 959–970. [CrossRef]
6. Desmurs, L.; Manatschal, G.; Bernoulli, D. The Steinmann Trinity Revisited: Mantle Exhumation and Magmatism along an Ocean-continent Transition: The Platta Nappe, Eastern Switzerland. In *Non-Volcanic Rifting of Continental Margins: A Comparison of Evidence from Land and Sea*; Wilson, R.C.L., Whitmarsh, R.B., Taylor, B., Froitzheim, N., Eds.; Geological Society of London: London, UK, 2001; Volume 187, pp. 235–266.
7. Kelley, D.S.; Karson, J.A.; Früh-Green, G.L.; Yoerger, D.R.; Shank, T.M.; Butterfield, D.A.; Hayes, J.M.; Schrenk, M.O.; Olson, E.J.; Proskurowski, G.; et al. A Serpentinite-Hosted Ecosystem: The Lost City Hydrothermal Field. *Science* **2005**, *307*, 1428–1434. [CrossRef]
8. Ludwig, K.A.; Kelley, D.S.; Butterfield, D.A.; Nelson, B.K.; Früh-Green, G. Formation and evolution of carbonate chimneys at the Lost City Hydrothermal Field. *Geochim. Cosmochim. Acta* **2006**, *70*, 3625–3645. [CrossRef]
9. Früh-Green, G.L.; Connolly, J.A.; Plas, A.; Kelley, D.S.; Grobéty, B. Serpentinization of oceanic peridotites: Implications for geochemical cycles and biological activity. *Subseafloor Biosph. Mid-Ocean. Ridges* **2004**, *144*, 119–136.
10. Boschi, C.; Dini, A.; Früh-Green, G.L.; Kelley, D.S. Isotopic and element exchange during serpentinization and metasomatism at the Atlantis Massif (MAR 30 N): Insights from B and Sr isotope data. *Geochim. Cosmochim. Acta* **2008**, *72*, 1801–1823. [CrossRef]
11. Kerrick, D. Serpentinite seduction. *Science* **2002**, *298*, 1344–1345. [CrossRef]
12. Pereira, D.; Yenes, M.; Sánche, J.; Moreno, M. Characterization of serpentinites to define their appropriate use as dimension stone. *Geol. Soc. Lond. Spec. Publ.* **2007**, *271*, 55–62. [CrossRef]
13. Pereira, D.; López, A.J.; Ramil, A.; Bloise, A. The importance of prevention when working with hazardous materials in the case of serpentinite and asbestos when cleaning monuments for restoration. *Appl. Sci.* **2023**, *13*, 43. [CrossRef]
14. Melfos, V. Green Thessalian stone: The byzantine quarries and the use of a unique architectural material from the Larisa area, Greece. Petrographic and geochemical characterization. *Oxf. J. Archaeol.* **2008**, *27*, 387–405. [CrossRef]
15. Pereira, D. A report on serpentinites in the context of heritage stone resources. *Episodes* **2012**, *35*, 478–480. [CrossRef] [PubMed]
16. Cavallo, A.; Rimoldi, B. Chrysotile asbestos in serpentinite quarries: A case study in Valmalenco, Central Alps, Northern Italy. *Environ. Sci. Process. Impacts* **2013**, *15*, 1341–1350. [CrossRef] [PubMed]
17. Cavallo, A. Serpentinitic waste materials from the dimension stone industry: Characterization, possible reuses and critical issues. *Resour. Policy* **2018**, *59*, 17–23. [CrossRef]
18. Cavallo, A. Serpentino della Valmalenco (Central Alps, Northern Italy): A green dimension stone with outstanding properties. *Resour. Policy* **2022**, *75*, 102467. [CrossRef]
19. Punturo, R.; Cirrincione, R.; Pappalardo, G.; Mineo, S.; Fazio, E.; Bloise, A. Preliminary laboratory characterization of serpentinite rocks from Calabria (southern Italy) employed as stone material. *J. Mediterr. Earth Sci.* **2018**, *10*, 79–87.
20. Nespereira, J.; Navarro, R.; Monterrubio, S.; Yenes, M.; Pereira, D. Serpentinite from Moeche (Galicia, Northwestern Spain). A stone used for centuries in the construction of the architectural heritage of the region. *Sustainability* **2019**, *11*, 2700. [CrossRef]
21. Fratini, F.; Rescic, S.; Pittaluga, D. Serpentinite and ophicalcite in the architecture of eastern Liguria and as decoration of Tuscan religious buildings. *Resour. Policy* **2022**, *75*, 102505. [CrossRef]

22. Faraj, R.Q. Evaluation of the Waras Serpentinite Rocks for Dimension Stone, Mawat Ophiolite Complex, Kurdistan Region, NE Iraq. *Tikrit J. Pure Sci.* **2023**, *27*, 43–50. [CrossRef]
23. Punturo, R.; Bloise, A.; Critelli, T.; Catalano, M.; Fazio, E.; Apollaro, C. Environmental implications related to natural asbestos occurrences in the ophiolites of the Gimigliano-Mount Reventino Unit (Calabria, southern Italy). *Int. J. Environ. Res.* **2015**, *9*, 405–418.
24. Bloise, A.; Critelli, T.; Catalano, M.; Apollaro, C.; Miriello, D.; Croce, A.; Barrese, E.; Liberi, F.; Piluso, E.; Rinaudo, C.; et al. Asbestos and other fibrous minerals contained in the serpentinites of the Gimigliano-Mount Reventino Unit (Calabria, S-Italy). *Environ. Earth Sci.* **2014**, *71*, 3773–3786. [CrossRef]
25. Bloise, A.; Catalano, M.; Critelli, T.; Apollaro, C.; Miriello, D. Naturally occurring asbestos: Potential for human exposure, San Severino Lucano (Basilicata, southern Italy). *Environ. Earth Sci.* **2017**, *76*, 1–13. [CrossRef]
26. Dichicco, M.C.; Castiñeiras, P.; Galindo Francisco, C.; González Acebrón, L.; Grassa, F.; Laurita, S.; Paternoster, M.; Rizzo, G.; Sinisi, R.; Mongelli, G. Genesis of carbonate-rich veins in the serpentinites at the Calabria-Lucania boundary (southern Apennines). *Rend. Online Soc. Geol.* **2018**, *44*, 143–149. [CrossRef]
27. Dichicco, M.C.; Paternoster, M.; Rizzo, G.; Sinisi, R. Mineralogical asbestos assessment in the southern Apennines (Italy): A review. *Fibers* **2019**, *7*, 24. [CrossRef]
28. Bloise, A.; Ricchiuti, C.; Giorno, E.; Fuoco, I.; Zumpano, P.; Miriello, D.; Apollaro, C.; Crispini, A.; De Rosa, R.; Punturo, R. Assessment of naturally occurring asbestos in the area of Episcopia (Lucania, Southern Italy). *Fibers* **2019**, *7*, 45. [CrossRef]
29. Rizzo, G.; Dichicco, M.C.; Castiñeiras, P.; Grassa, F.; Laurita, S.; Paternoster, M.; Sinisi, R.; Mongelli, G. An Integrated Study of the Serpentinite-Hosted Hydrothermal System in the Pollino Massif (Southern Apennines, Italy). *Minerals* **2020**, *10*, 127. [CrossRef]
30. Ricchiuti, C.; Pereira, D.; Punturo, R.; Giorno, E.; Miriello, D.; Bloise, A. Hazardous elements in asbestos tremolite from the Basilicata region, southern Italy: A first step. *Fibers* **2021**, *9*, 47. [CrossRef]
31. Cavalcante, F.; Belviso, C.; Finizio, F.; Lettino, A.; Fiore, S. *Geological Map of Liguride Unit Area of the Pollino (Basilicata Region): New Data Geological, Mineralogical and Petrographic*; Fiore, S., Ed.; Digilabs: Bari, Italy, 2009; ISBN 978-88-7522-026-6.
32. Knott, S.D. The Liguride Complex of Southern Italy—A Cretaceous to Paleogene accretionary wedge. *Tectonophysics* **1987**, *142*, 217–226. [CrossRef]
33. Monaco, C.; Tortorici, L. Tectonic role of ophiolite-bearing terrains in the development of the Southern Apennines orogenic belt. *Terra Nova* **1995**, *7*, 153–160. [CrossRef]
34. Tortorici, L.; Catalano, S.; Monaco, C. Ophiolite-bearing mélanges in southern Italy. *Geol. J.* **2009**, *44*, 153–166. [CrossRef]
35. Critelli, S.; Le Pera, E. Post-Oligocene sediment-dispersal system and unroofing history of the Calabrian microplate, Italy. *Int. Geol. Rev.* **2009**, *40*, 609–637. [CrossRef]
36. Liberi, F.; Morten, L.; Piluso, E. Geodynamic significance of ophiolites within the Calabrian Arc. *Island Arc.* **2006**, *15*, 26–43. [CrossRef]
37. Spadea, P. I carbonati delle rocce metacalcaree della Formazione del Frido della Lucania. *Ofioliti* **1976**, *1*, 431–465.
38. Laurita, S.; Cavalcante, F.; Belviso, C.; Prosser, G. The Liguride Complex of the Pollino area (southern Apennines): Tectonic setting and preliminary mineralogical data. *Rend. Online Soc. Geol.* **2008**, *2*, 1–3.
39. Sansone, M.T.C.; Prosser, G.; Rizzo, G.; Tartarotti, P. Spinel peridotites of the Frido unit ophiolites (southern Apennines Italy): Evidence for oceanic evolution. *Period. Mineral.* **2012**, *81*, 35–59.
40. Cirrincione, R.; Fazio, E.; Fiannacca, P.; Ortolano, G.; Pezzino, A.; Punturo, R. The Calabria-Peloritani Orogen, a composite terrane in Central Mediterranean; its overall architecture and geodynamic significance for a pre-Alpine scenario around the Tethyan basin. *Period. Mineral.* **2015**, *84*, 701–749.
41. Sansone, M.T.C.; Rizzo, G. Pumpellyite veins in the metadolerite of the Frido unit (southern Apennines-Italy). *Period. Mineral.* **2012**, *81*, 75–92.
42. Dichicco, M.C.; Laurita, S.; Paternoster, M.; Rizzo, G.; Sinisi, R.; Mongelli, G. Serpentinite Carbonation for CO_2 Sequestration in the Southern Apennines: Preliminary Study. *Energy Procedia* **2015**, *76*, 477–486. [CrossRef]
43. Rizzo, G.; Buccione, R.; Paternoster, G.; Laurita, S.; Bloise, L.; Calabrese, E.; Sinisi, R.; Mongelli, G. Geochemistry and petrology of leucocratic rocks in the ophiolites from the Pollino Massif (Southern Italy): Origin and tectonic significance. *Minerals* **2021**, *11*, 1264. [CrossRef]
44. Boskabadi, A.; Pitcairn, I.K.; Broman, C.; Boyce, A.; Teagle, D.A.; Cooper, M.J.; Azer, M.K.; Stern, R.J.; Mohamed, F.H.; Majka, J. Carbonate alteration of ophiolitic rocks in the Arabian–Nubian Shield of Egypt: Sources and compositions of the carbonating fluid and implications for the formation of Au deposits. *Int. Geol. Rev.* **2017**, *59*, 391–419. [CrossRef]
45. Mongelli, G.; Cullers, R.L.; Dinelli, E.; Rottura, A. Elemental mobility during the weathering of exposed lower crust: The kinzigitic paragneisses from the Serre, Calabria, southern Italy. *Terra Nova* **1998**, *10*, 190–195. [CrossRef]
46. Punturo, R.; Ricchiuti, C.; Bloise, A. Assessment of serpentine group minerals in soils: A case study from the village of San Severino Lucano (Basilicata, Southern Italy). *Fibers* **2019**, *7*, 18. [CrossRef]
47. Barnes, I.; O'Neil, J.R. The relationship between fluids in some fresh alpine-type ultramafics and possible modern serpentinization, Western United States. *Geol. Soc. Am. Bull.* **1969**, *80*, 1947–1960. [CrossRef]
48. Neal, C.; Stanger, G. Hydrogen generation from mantle source rocks in Oman. *Earth Planet. Sci. Lett.* **1983**, *66*, 315–320. [CrossRef]
49. Papastamaki, A. The alkalinity and the chemical composition of springs issuing from peridotites. *Ann. Géol. Des. Pays. Hell.* **1977**, *28*, 551–556.

50. Robles-Camacho, J.; Armienta, M.A. Natural chromium contamination of groundwater at León Valley, México. *J. Geochem. Explor.* **2000**, *68*, 167–181. [CrossRef]
51. Goyer, R.A. Results of lead research: Prenatal exposure and neurological consequences. *Environ. Health Perspect.* **1996**, *104*, 1050–1054. [CrossRef]
52. Katz, S.A.; Salem, H. The toxicology of chromium with respect to its chemical speciation: A review. *J. Appl. Toxicol.* **1993**, *13*, 217–224. [CrossRef]
53. Kortenkamp, A.; Casadevall, M.; Faux, S.P.; Jenner, A.; Shayer, R.O.; Woodbridge, N.; O'Brien, P. A role for molecular oxygen in the formation of DNA damage during the reduction of the carcinogen chromium (VI) by glutathione. *Arch. Biochem. Biophys.* **1996**, *329*, 199–207. [CrossRef]
54. Bartlett, R.; James, B. Behavior of chromium in soils: III. Oxidation. American Society of Agronomy. *Crop Sci. Soc. Am. Soil Sci. Soc. Am.* **1979**, *8*, 31–35.
55. Eary, L.E.; Rai, D. Kinetics of chromium (III) oxidation to chromium (VI) by reaction with manganese dioxide. *Environ. Sci. Technol.* **1987**, *21*, 1187–1193. [CrossRef]
56. Fendorf, S.E. Surface reactions of chromium in soils and waters. *Geoderma* **1995**, *67*, 55–71. [CrossRef]
57. Oze, C.; Fendorf, S.; Bird, D.K.; Coleman, R.G. Chromium geochemistry in serpentinized ultramafic rocks and serpentine soils from the Franciscan complex of California. *Am. J. Sci.* **2004**, *304*, 67–101. [CrossRef]
58. Wittbrodt, P.R.; Palmer, C.D. Reduction of Cr (VI) in the presence of excess soil fulvic acid. *Environ. Sci. Technol.* **1995**, *29*, 255–263. [CrossRef]
59. Wittbrodt, P.R.; Palmer, C.D. Effect of temperature, ionic strength, background electrolytes, and Fe (III) on the reduction of hexavalent chromium by soil humic substances. *Environ. Sci. Technol.* **1996**, *30*, 2470–2477. [CrossRef]
60. Decreto Legislativo 3 Aprile 2006, n. 152, Norme in Materia Ambientale, 2006. Available online: https://www.normattiva.it/uri-res/N2Ls?urn:nir:stato:decreto.legislativo:2006-04-03;152 (accessed on 3 April 2006).
61. Kierczak, J.; Neel, C.; Bril, H.; Puziewicz, J. Effect of mineralogy and pedoclimatic variations on Ni and Cr distribution in serpentine soils under temperate climate. *Geoderma* **2007**, *142*, 165–177. [CrossRef]
62. Oze, C.; Bird, D.K.; Fendorf, S. Genesis of hexavalent chromium from natural sources in soil and groundwater. *Proc. Natl. Acad. Sci. USA* **2007**, *104*, 6544–6549. [CrossRef]
63. Boccia, P.; Meconi, C.; Sturchio, E.; Margiotta, S.; Ragone, P.; Summa, V. Natural geochemical risk in the Pollino Massif: A case-study of chromium. In Proceedings of the ICAW 2015—11th International Comet Assay Workshop, Antwerpen, Belgium, 1–4 September 2015; Volume 115, pp. 1–12.
64. Margiotta, S.; Mongelli, G.; Summa, V.; Paternoster, M.; Fiore, S. Trace element distribution and Cr(VI) speciation in Ca-HCO3 and Mg-HCO_3 spring waters from the northern sector of the Pollino massif, southern Italy. *J. Geochem. Explor.* **2012**, *115*, 1–12. [CrossRef]
65. Summa, V.; Boccia, P.; Lettino, A.; Margiotta, S.; Palma, A.; Ragone, P.P.; Sinisi, R.; Zanellato, M.; Sturchio, E. Mobility of trace metals in serpentinite-derived soils of the Pollino Massif (Southern Italy): Insights on bioavailability and toxicity. *Environ. Geochem. Health* **2020**, *42*, 2215–2232. [CrossRef] [PubMed]
66. IARC Monographs Programme on the Evaluation of the Carcinogenic Risk of Chemicals to Humans. In *Some Industrial Chemicals*; World Health Organization International Agency for Research on Cancer: Lyon, France, 2000; Volume 77, p. 563.
67. World Health Organization. *Cancer Pain Relief*; World Health Organization: Geneva, Switzerland, 1986; p. 74. ISBN 92-4-156100-9.
68. DM 18/03/2003 Regolamento per la Realizzazione di una Mappatura delle Zone del Territorio Nazionale Interessate Dalla Presenza di Amianto, ai Sensi Dell'articolo 20 della Legge 23 Marzo 2001, n. 93, 2003. Available online: https://www.google.com/url?sa=t&rct=j&q=&esrc=s&source=web&cd=&ved=2ahUKEwjBocnk7b-BAxUI0GEKHZ1WACcQFnoECA0QAQ&url=https%3A%2F%2Fwww.sardegnasalute.it%2Fdocumenti%2F9_463_20150211095806.pdf&usg=AOvVaw0z5No6NE0rZWrqG-rSueWP&opi=89978449 (accessed on 1 August 2023).